Supporting Information (SI)

Fabrication of the novel mixed matrix Polymer Electrolyte Membranes (PEMs) intended for renewable hydrogen production via electrolysis application

Relebohile Mokete[1*], František Mikšík[2,3], Roman Selyanchyn[2], Nobuo Takata[1], Kyaw Thu[1,2], Takahiko Miyazaki[1,2]

1 Department of Energy and Environmental Engineering, Interdisciplinary Graduate School of Engineering Sciences, Kyushu University, 6-1 Kasuga-koen, Kasuga-shi, Fukuoka 816-8580, Japan
2 Research Center for Next Generation Refrigerant Properties (NEXT-RP), International Institute of Carbon-Neutral Energy Research (I2CNER), Kyushu University, 744 Motooka, Nishi-ku, Fukuoka 819-0395, Japan
3 Institute of Innovation for Future Society, Nagoya University Furu-cho, Chikusa, Nagoya 464-8603, Japan

*Corresponding author email: relemokete@kyudai.jp

1. Thermodynamic parameters and efficiency determination

The thermodynamic parameters involved in water electrolysis (WE) such as change in enthalpy (ΔH^o), Gibbs free energy (ΔG^o), and entropy ($T\Delta S^o$) depict the amount of energy required for water electrolysis. This includes the minimum reversible work necessary to split water and the thermal energy that is unavailable to participate in the reaction but rather supplied as heat [1, 2]. The relationship between these parameters is shown in equation S1 and can be further associated with water, hydrogen, and oxygen as ideal gases at standard conditions (temperature = 298 K and pressure = 10^5 Pascal) where ΔH^o = 286 kJ mol^{-1} and ΔG^o = 237 kJ mol^{-1} [3, 4].

$$\Delta H^o = \Delta G^o + T\Delta S^o \quad \text{S1}$$

Therefore, the reversible voltage (V_{rev}) that drives water splitting can be calculated using ΔG^o (equation S2), where n and F are respectively the numbers of transferred charges for each H_2 molecule (n = 2) and F is Faraday's constant (F = 96 485 C mol^{-1}). When the conditions are not ideal, the atmospheric pressure and temperature of electrolyzers are usually below 80 °C, hence, some extra energy is required for water splitting. The thermoneutral potential is used to express the energy that corresponds to the reversible potential. Therefore, the expression of thermoneutral potential (V_{tn}) is represented in terms of ΔH^o by equation S3 where n and F imply similar parameters mentioned previously [2, 4].

$$V_{rev} = \frac{\Delta G^o}{nF} = \frac{237000}{2 \times 96485} = 1.23\text{V} \quad \text{S2}$$

$$V_{tn} = \frac{\Delta H^o}{nF} = \frac{286000}{2 \times 96485} = 1.48\text{V} \quad \text{S3}$$

The electrolyzer's voltage is commonly expressed according to equation S4 where V_{act}, $V_{ohm,}$ and E represent activation polarization, ohmic polarization, and open-circuit voltage, respectively. Therefore, E is calculated with respect to equation 8 where R, $T_{elec.}$, F, and a_{H_2O} symbolise universal gas constant, Faraday's constant, the temperature of the electrolyzer, and water activity between the anode and electrolyte, respectively [5-7]:

$$V_{elec} = V_{act} + V_{ohm} + E \quad \text{S4}$$

$$E = E_0 + \frac{RT_{elec.}}{2F} \ln\left(\frac{P_{H_2} \times P_{O_2}^{0.5}}{a_{H_2O}}\right) \quad \text{S5}$$

E_0 (V_{rev}) is the standard voltage calculated following equation S2. The activation potential is denoted by equation S6. Here, i, i_o and α refer to current density, exchange current density and charge transfer coefficient, respectively. The membrane resistance and ohmic potential are also denoted by equations S7 and S8, where σ_m and t_m represent membrane conductivity as well as thickness, respectively [6].

$$V_{act} = V_{rev} + \frac{RT_{elec.}}{2F} \ln\left(\frac{i}{i_o}\right) \quad \text{S6}$$

$$R_{ohm} = \frac{t_m}{\sigma_m} \quad \text{S7}$$

$$V_{\Omega} = iR_{ohm} \quad \text{S8}$$

The energy efficiency (η_{eff} %) of a cell can be calculated based on the energy provided from the H_2 production and expressed in terms of the higher heating

value of H_2 (HHV_{H_2}) divided by the consumed energy which is a product of current (I), voltage (V) and the time (t) it took for H_2 to be produced (Equation S9) [2].

$$\eta_{eff}\,\% = \frac{moles\ H_2\ produced\ \times\ HHV_{H2}}{I \times V \times t} \times 100\% \qquad \text{S9}$$

The energy efficiency (η_{energy} %) is also calculated by the ratio between the energy content of H_2 and the amount of electrical energy necessary (Equation S10). In equation S10, H_{H_2} (equivalent to 11 929 kJ/m^3) represents the calorific value of H_2 at temperature = 20^{o}C, I is current in mA, t is time (seconds) and V_{H_2} is the experimental volume of H_2 (mL) [8, 9].

$$\eta_{energy}\,\% = \frac{H_{H_2} \times V_{H2\ experimental}}{U \times I \times t} \times 100\% \qquad \text{S10}$$

2. PEM transformation during fabrication

The transformation of the membranes during preparation is represented by CT-M in Fig S1. The dried PEMs before cross-linking looked transparent (Fig. S1. a), but they became dark brown and opaque immediately after cross-linking (Fig. S1. b), whereas the reacted membranes still maintained their structure (Fig. S1. c).

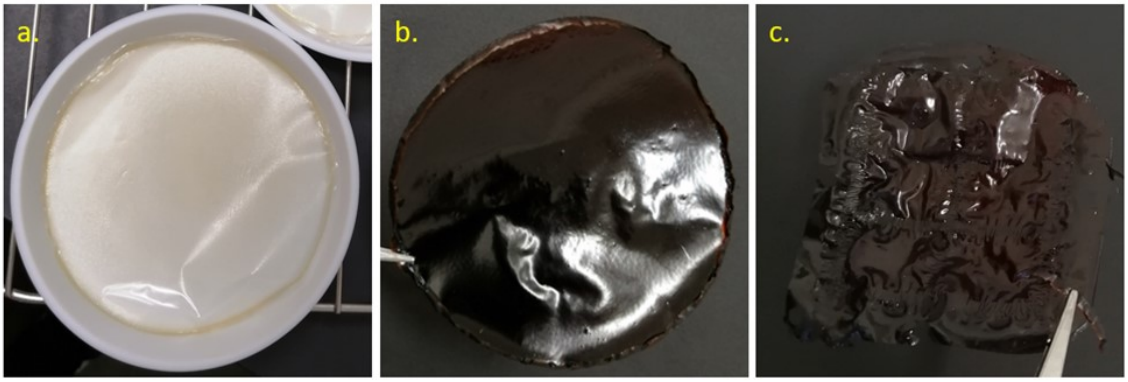

Fig. S1. The representative membrane for the fabricated PEMs after drying but before cross-linking (a), after cross-linking (b) and after electrolysis experiment (c). Fabricated PEM parameters: matrix: PVA-PVP (1:1), cross-linker: SSA, cross-linking temperature (°C): 120, cross-linking time (hours): 3, drying temperature (°C): 40, drying time (hours): 24, filler: CT

3. FT/IR

The FT/IR spectrum identification is on Table S1.

Table S1: FT/IR spectra identification

Peak identification Group	Wavenumber (cm^{-1})	
	Current study	Reference study
O-H (hydroxyl group)	3386 3591	1423–1417 [10] 3300 [11] 3320 [12] 3342 [13] 3000-3600 [14] 3350-3500 [15] 3700-3200 [10]
C-H (alkyl group)	862 2920 2965 1126	1115 [11], 2850, 2950 [11] 2910 [16],2928[12,13], 2920 [14] 1000-500 [10] 844, 2942 [16] 897 [17]
C-O (alkyl phenol group)	1030 1043 1047 1226	1040 [11] 1021 [13] 1035, 1281 [12] 1033 [14] 1091 [16] 1213 [15] 1223, 1247 [18]
C=O (carbonyl, carboxylic groups)	1269 1604 1740	1270 [4 13], 1631 [4],1635 [5 14] 1740-1610 [10] 1656, 1721 [16]
C=C (alkene)	1509	1601, 1512 [12,18] 1650-1500 [10]

-CH_2 (methylene group)	-	1415 [16] 1426 [17]
-CH_3 (methyl group)	-	1331 [16]
-SO_3 (sulfonic acid group)	-	1250 [19] 1100-1250 [20]

4. Water physisorption isotherms

The water adsorption (physisorption) isotherm classification is according to Table S2 [21-23].

Table S2: Physisorption Isotherms Classification

Isotherm	Characterization	Illustration
Type I	■ Concave to P/P_0 ■Pore accessibility limits water uptake instead of the internal surface ■ Exhibited by microporous adsorbents (narrow micropores; type I(a) and wider micropores type I(b) ■e.g activated carbon, Zeolite, porous oxides)	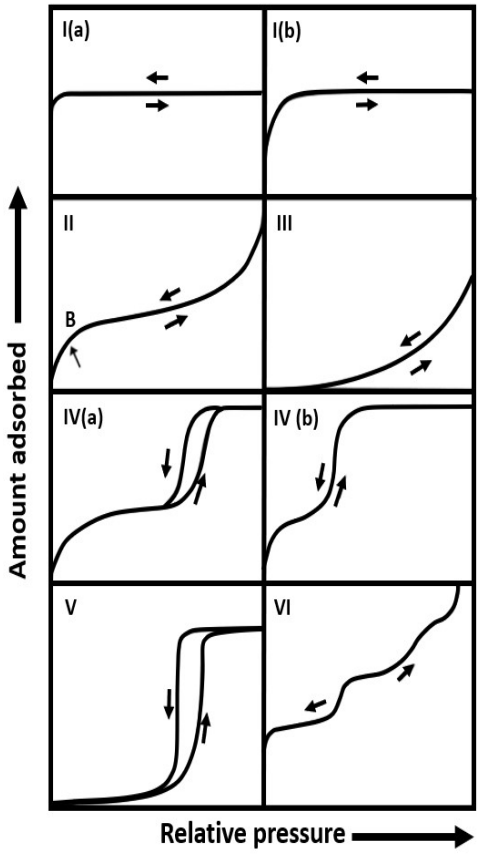
Type II	■ Happens in non-porous or macroporous adsorbents ■ Monolayer occurs and multilayer sorption happens at a higher relative pressure ■e.g non-porous alumina and silica	

Type III	■ Materials exhibiting weak adsorbate and adsorbent interactions ■ No monolayer formation ■ Adsorbed molecules clustered around sites preferable surface sites ■e.g (Graphite and water)
Type IV	■ Occurs in mesoporous and non-porous materials ■ Capillary condensation is followed by hysteresis (type IV(a) and smaller width adsorbents undergo type IV(b) ■ Multilayer sorption manifests ■e.g (Mesoporous alumina and silica)
Type V	■Exhibited by both hydrophobic microporous and mesoporous materials with weak adsorbate and adsorbent interactions ■e.g Activated carbon, water
Type VI	■Involves sequential multi-layer sorption on homogeneous surface materials ■e.g Graphite/Krypton or Graphite/argon

102

103

5. Membrane characterization

5. 1 Proton conductivity comparison

For the proton conductivity comparison, many studies reported various values depending on the study aim. For instance, Liu et al. [24] developed the low-cost PEMs for direct methanol adsorption. The PEMs were fabricated using a blend of PVA/HFA (PVA/hexafluoroglutaric acid) plus BASANa (Benzenesulfonic acid sodium salt) and GA (Glutaraldehyde) as binary reaction agents. The range of the proton conductivity obtained from Liu et al.'s study [24] was within the range of 10^{-3} to 10^{-2} S/cm and the fabricated PEMs exhibited lower proton conductivity compared to that of Nafion™ 115. According to the literature, Ebenezer et al [25] reported the proton conductivity of the Nafion™ 115 membrane to be 0.14 S/cm under humidified conditions whereas it was 0.1 S/cm at room temperature while that of PVA-SSA was 0.077 S/cm under humidified conditions [25]. In another study by Kamaroddin et al [26], Nafion exhibited the proton conductivity of 10.06 mS/cm at 90 ^{o}C. A study by Kamjornsupamitr et al. [27] found the proton conductivity of the glutaraldehyde (0.5M) cross-linked PVA/SSA (molar ratio 1:0.2) to be 0.034 S/cm while that of Nafion at 30 ^{o}C and 100% relative humidity was 0.1 S/cm which was the highest comparatively. Furthermore, PVA/SSA membranes prepared by Rhim et al. [28] had ~~the~~ proton conductivities in the range of 10^{-2} - 10^{-3} S/cm. In another study by Tasarin et al. [29], the pristine PVA-SSA had the proton conductivity of 2.7 mS/cm and 2.3 mS/cm at the respective temperatures of 27 ^{o}C and 80 ^{o}C under non-humidified conditions. According to Zhu et al. [30], the proton conductivities of the water molecules plus sulfonic acid groups are around 10 – 100 mS/cm while the activation energy is around 0.1 and 0.5 eV because of hydration levels.

5. 2 Ion Exchange capacity (IEC), water uptake (WU) and swelling ratio (SR)

In addition to the water adsorption experiments, the ion exchange capacity (IEC), water uptake (WU) based on mass change and swelling ratio (SR) with respect to thickness were determined (Fig. S3). NF-M had the lowest values of the IEC (1.2 meq. g^{-1}), WU (11%), and SR (19.9%) whereas PB (IEC = 4.1 meq. g^{-1}, WU = 133.7%, and SR = 34.4%) outperformed SSA-M (IEC = 1.8 meq. g^{-1}, WU = 121.7% and SR = 26.4%) and CT (IEC = 2.3

meq. g^{-1}, WU = 114% and SR = 22.1%) respectively. The IEC, WU based on mass % change and thickness-related SR for the fabricated PEMs were analysed and the results are reported below (Fig. S3). The comparison of WU, SR and IEC for NF with other studies in shown on Table S3, and the reported IEC is 0.89-1.3 meq. g^{-1}, WU is 7.3-31.5%, while the SR is 30-53.9% but the results vary depending on the NF membrane type, thickness and temperature conditions [31-34]. A very interesting outcome is that of CT-M where the IEC was higher than that of SSA-M, but the WU and SR were the least (Fig. S3). Accordingly, the least WU and SR of the CT-M may be attributed to a combination of intense hydrophilicity of the terminal sulfonic acid groups on the polymer backbone and the degree of hydrophobicity within the PEM, which results in hydrophilic/hydrophobic separation on the surface [34]. After the incorporation of fillers, there is a reduction of sulfonic groups but the incorporation of additional groups from the filler, so the filler properties also play a role in determining the WU and water retention. Thus in the case of CT-M, the proton transport via vehicular mechanism was affected in the presence of the filler [33]. Although WU and SR are associated with proton conduction, orientation of internal and terminal groups also determines the degree of transport within the PEM as well as the hydrophilicity of the functional groups [34].

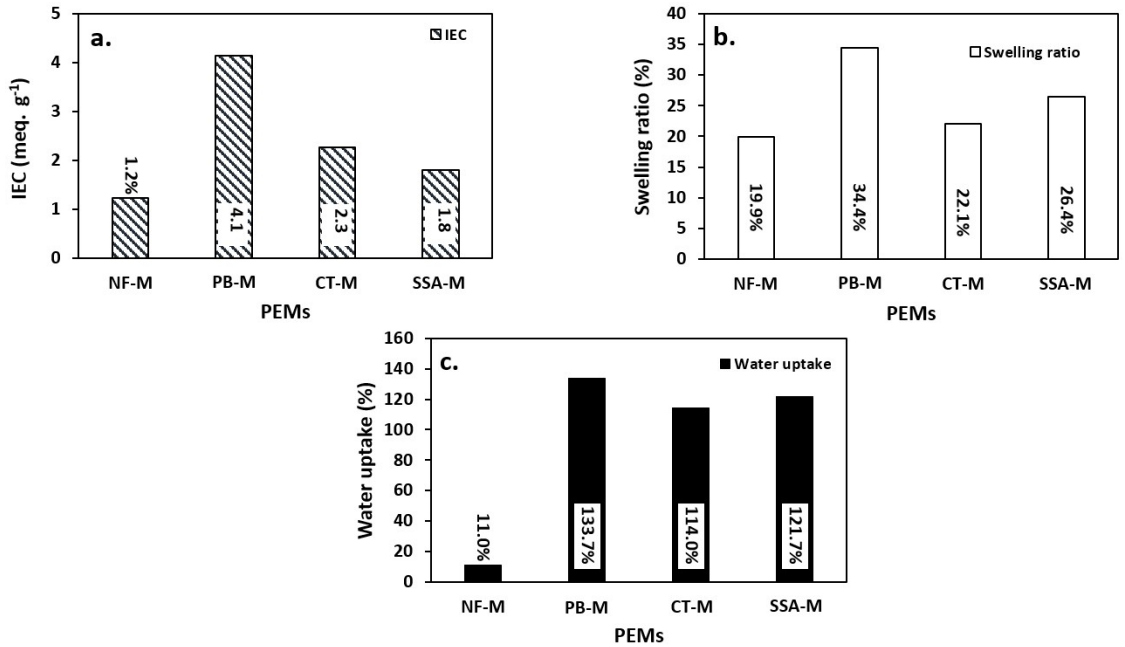

Fig. S3. Water uptake and swelling ratio of the PEMs: NF, PB, CT and SSA. Experimental parameters: titrate: NaCl (1M), titrant: NaOH (0.1M), PEMs drying temperature (^oC): 70, soaking time in DI water (hour): 4, PEMs' area (cm^2): 1

Comparison with the literature was also done and the reference results are shown in table S3.

Table S3: Comparison of IEC, water uptake and swelling ratio of the PEMs from the literature

PEM	Temp. (^oC)	WU (%)	SR (%)	IEC (meq. g^{-1})	T (µm)	PC (mS/cm)
NF211 [31]	30	7.3	30.0	0.89	25	70
	90	18.1	53.9	0.89	25	135.6
NF212[16]	25	-	-	-	0.02	0.125
[35]	100	-	-	-	-	100
NF117 [34]	25	28.51	-	0.91		29.5
NF (5% wt solution) [33]	110	18	-	1.3	-	1.8
NF112 [32]	-	-	-	0.91	80	-
NF115 [32]	-	-	-	0.91	125	-
NF117 [32]	-	31.5	-	0.91	175	100
NMPC/PVA [35]	-	51	-	0.56	-	-
PVA [36]	-	50.73	18	0.25	24	-
PVA/SSA [29]	27	-	-	2.25	-	2.7

PVA/SSA [25]	25	-	-	-	200	77
PVA/SSA [27]	27	54.6	-	3.49		34.4
PVA/HFA [24]	<60 >60	25.12-160.9	-	0.632-1.158 0.621-1.043	100-250	14.2-62.7 13.9-56.3

Proton Exchange Membrane (PEM), Temperature (Temp.), Water uptake (WU), swelling ratio (SR), Ion exchange capacity (IEC), Thickness (T) and Proton conductivity (PC), Nafion (NF), N-methylene phosphonic chitosan/poly vinyl alcohol (NMPC/PVA), poly (vinyl alcohol)/hexafluoroglutaric acid (PVA/HFA), references are written in brackets [].

6. Mechanical properties

Some physico-mechanical properties include tensile strength (TS), tensile modulus (TM) as well as elongation break (EB). Therefore, in correspondence to the manufacturer's specifications (Fuel cell Earth), NF-M had the TS, TM and EB of 43 MPa, 249 MPa, and 1.98% respectively at 50% relative humidity and 23 ^{o}C [37]. The PVA-PVP-SSA cross-linked PEMs had the respective TS, TM and EB of 60 MPa, 2.1 MPa and EB of 3.2% [38]. The TS of the membranes is higher than that of Nafion™ 115, consistent with the findings from other studies [39]. The higher tensile strength implies increased rigidity of the PEM [40]. Also, the more porous the material, the lower the tensile strength and the more ductile it becomes [41]. In a typical PVA-SSA PEM application study, the TS and EB of PVA-SSA to be 145 MPa and 24.7% respectively [41].

7. Gel fraction

The gel fraction (GF) is a measure of the degree of cross-linking within the polymer network [42]. It is ~~regarded~~ considered ~~as the~~ insoluble membrane, while the swollen polymer part upon contact with the solvent is known as the SR [43].

To determine the gel fraction, following Elzubair et al. [43] and Gulenoor et al. [44], the PEM samples were cut into 1cm × 1cm and dried for 2 hours at 60 ^{o}C (W_a). They were then placed in DI water for 24 hours at 25 ^{o}C so as to get rid of the soluble fraction. Subsequently, the membranes were dried again at 60 ^{o}C for 2 hours (W_b). The gel fraction was calculated according to equation S11 below

[43, 44].

$$\text{Gel fraction (\%)} = \frac{W_b}{W_a} \times 100\% \qquad \text{S11}$$

Table S4: Gel fraction results of the fabricated PEMs

PEM	Gel Fraction (%)
SSA-M	75.5
PB-M	81.7
CT-M	78.9

The gel fractions of PB-M, CT-M and SSA-M were found to be 81.7%, 78.9%, and 75.5% respectively (Table S4). Comparatively, the degree of cross-linking in PB-M was higher due to the compact polymer network, leading to improved properties [42]. However, it has been revealed that high cross-linking does not always guarantee the best results because sometimes excessive crosslinking reduces the network penetration effects [39]. The material's properties also play a significant role as CT-M had a slightly lower GF, implying that the CT filler did not yield the best results. The Nafion's GF has been reported as 16% and this may be due to the nature of the membrane which is soft and gel-like as opposed to the rest of the membrane that are brittle when dehydrated [30, 42, 45].

8. Biofilter properties

The biofilter technology is based on the concept of absorption, adsorption or bio-oxidation by the biofilter media [46]. Therefore, the filler materials and the PEMs possess biofilter properties due to the presence of the functional sites [47]. Conseuently, the various compounds become absorbed on the moisture film of the biofilters, thus water is necessary to maintain the moisture [46, 47]. When tested, PB was found to have a smoke removal efficiency of 100% whereas the pine wood chips removed odour from the nursing pig house air by 74% [46, 47]. This demonstrates that PEMs can function as biofilters, and the FT/IR results, along with water vapour properties support the verification of biofilter properties in the PEMs due to the presence of functional sites. Further in-depth research is still needed to fully understand the biofilter properties of the PEMs.

9. Nafion's formula

The chemical formula of Nafion is shown in Fig. S4 [48].

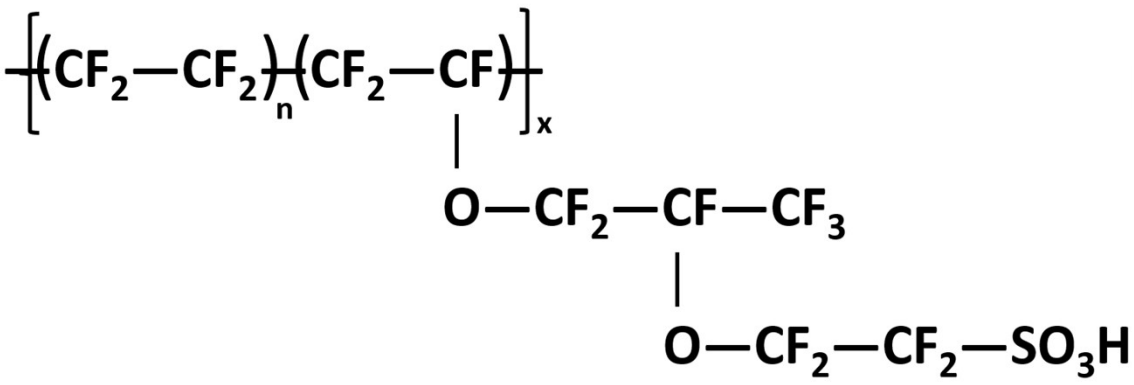

Fig. S4: Chemical formula of Nafion

10. Intrinsic properties of fillers

As aforementioned, the main fillers utilized include PB and CT. Considering their intrinsic properties, PB contains various phenolic compounds that determine its overall characteristics. Some of the phenolic compounds found in PB include catechin, ferulic acid, taxifolin and caffeic acid (Fig. S5 a-d)

[13]. The general properties of finely crushed PB (<10mm) and coarsely crushed PB (<20mm) are outlined in Table S5 [46].

Table S5: Intrinsic properties of PB

Property	Fine PB	Coarse PB
Air filled pores (%)	51	56
Bulk density (kg/m	0.34	0.44
Total nitrogen (mg N/g)	2.2	1.8

Based on the N_2 adsorption isotherms of PB at 77K, the specific surface area (S_{BET} (m^2/g)), pore volume (cm^3/g), average pore diameter (Å), real density (g/cm^3) and median particle size (mm) were 4.95, 0.006, 49.7, 1.1, and 0.152 respectively [13].

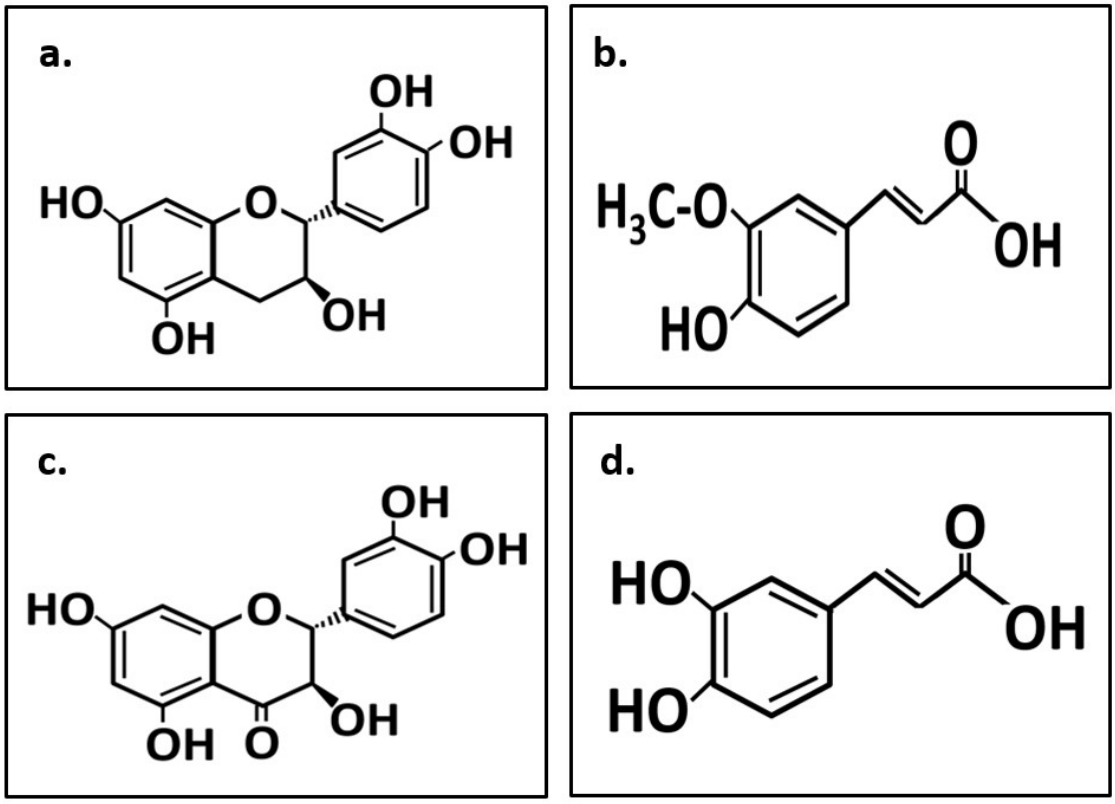

Fig. S5. Schemes of phenolic compounds extracted from PB including a. Catechin, b. Ferulic acid, c. Taxifolin, d. Caffeic acid

In terms of CT, the chemical extracts present in the seeds include hemicellulose (38.6%) and alpha-cellulose (18.9%) [49]. The CT seed capsule forms 22.81% of the whole seed [50]. Also, C- lignin is a biopolymer with strong acid resistance and it is a homogeneous linear polymer naturally found in plant seeds shells such as CT seeds [51].

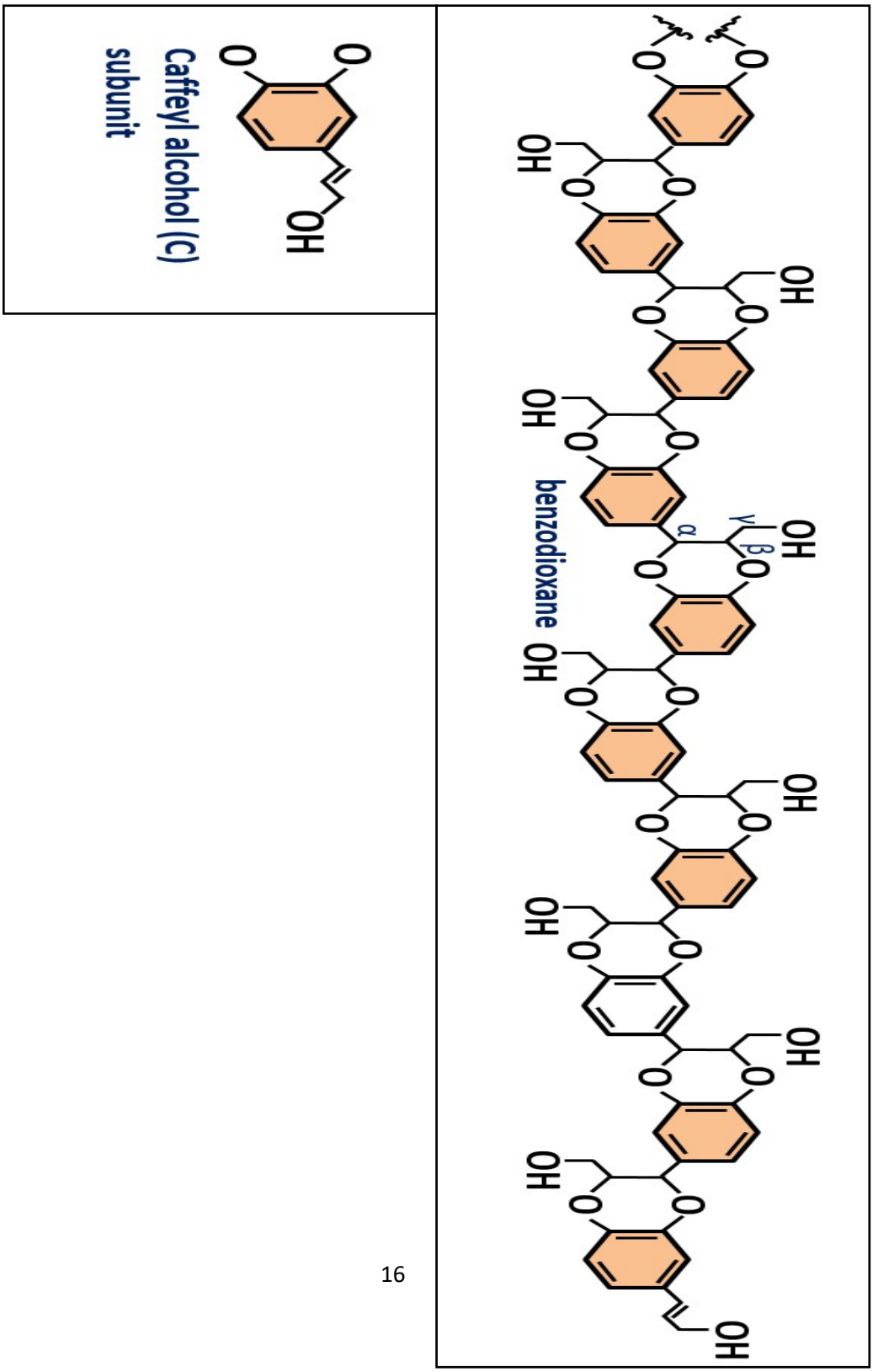

Fig. S6. The structure of C-lignin

11. Economics of the PEM electrolyzer

The economics of H_2 production by the PEM electrolyzer can be defined by the capital cost (C_{H_2}) [52, 53]. In this study, the capital costs include the cost of the electrolyzer (C_{elec}) plus that of the inserted PEM (C_{PEM}) as presented in equation S11 [54, 53]. The detailed costs of the electrolyzer and the materials used to fabricate the PEMs are shown in Table S6. The initial capital cost (C_{H_2}) normalized by the experimental hydrogen volume produced ($V_{H_2(produced)} = 4.77\ mL$) was calculated according to equation S12 and the C_{H_2} values are shown in Table S7 [55].

$$C_{H_2} = C_{elec} + C_{PEM} \quad \text{S11}$$

$$C_{H_2R} = \frac{C_{H_2}}{V\ (mL)} \quad \text{S12}$$

Table S6: Cost of the materials used for electrolysis

Materials	Quantity used	Rate ($)	Cost ($)
Electrolyzer (elec.)	1 elec.	163.77 $/elec.	163.77
Nafion 115	5.8cm × 4.6cm	0.18 $/cm^2	4.80
Polyvinyl alcohol (PVA)	5g	0.05 $/g	0.25
Polyvinyl pyrrolidone (PVP)	5g	0.13/g	0.65
Sulfoccinic acid (SSA)	2.45ml	0.44 $/ml	1.08

Asahi Silicon defoamer	0.5g	0.02 $/g	0.01
Water (PEM preparation + electrolysis)	500ml		
Fillers (CT and PB)	Obtained from their tree sources for free		

The normalized capital cost C_{H_2R} was reported with respect to the PEM inserted in the electrolyzer (Table S7). Electrolysis is costly when using NF-M as opposed to other PEMs (SSA-M, PB-M and CT-M). The economic cost for H_2 using NF-M was approximately 35.34 $/mL H_2 whereas that of the SSA-M, PB-M and CT-M was 34.75 $/mL H_2. These cost differences are mainly due to the fact that no filler was used in SSA-M whereas the fillers used in PB-M and CT-M were free because they were obtained directly from their respective trees. Comparatively, the fabricated PEMs were cheaper than the commercial NF-M, therefore they are recommended.

Table S7: Capital cost and normalized capital cost calculation based on PEM type used and experimental H_2 volume produced

Reactor	PEM type	Cost of Elec. + PEM ($)	C_{H_2} ($/mL H_2)
Electrolyzer (elec.)	NF-M	168.57	35.34
	SSA-M	165.76	34.75
	PB-M	165.76	34.75
	CT-M	165.76	34.75

12. SEM characterization for the electrodes

The results (Fig. S7) displayed and verified the manufacturer's specifications of the electrolyzer (Table 3 in the main text). Focusing on the H_2-producing electrode (cathode), Nickel was detected in a larger proportion (94.3 wt%, Fig. S7. c). For the O_2 electrode, small spherical and chain-like particles are visible on the surface, they mainly the platinum particles on the titanium surface (Fig. S7. d and e). These SEM results are in correspondence to the manufacturer's information, which indicated that nickel and platinum-plated titanium were used as cathode and anode materials respectively (Table 3 in the main text).

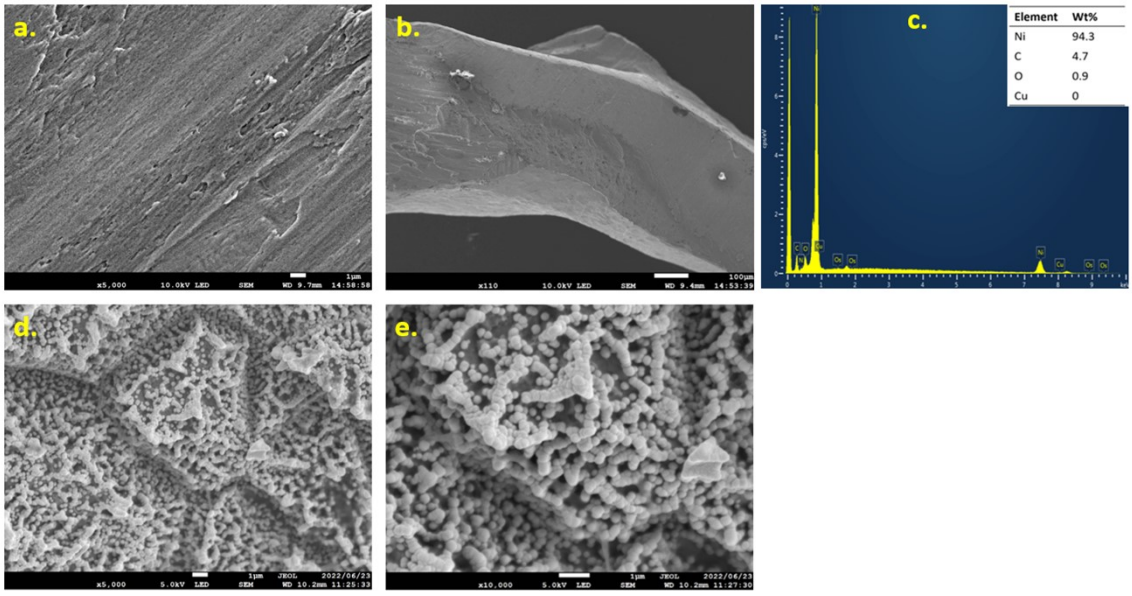

Fig. S7. SEM images of the electrodes including cathode (a and b) and EDX of the cathode (d) as well as the anode SEM images (d and e) at resolutions of 1µm and 100 µm

13. PV powered electrolysis

In the case where the power source is a PV cell, additional to the PV cell efficiency is defined by the ratio of the power output (P_{out}) to that of the power input (P_{in}) whereby P_{in} is the irradiance (IR = 1000 W/m^2) and cell area product (CA) [56, 57].

$$\eta_{SP} = \frac{P_{out}}{P_{in}} = \frac{P_{max}}{P_{in}} = \frac{P_{max}}{P_{in}} = \frac{P_{max}}{I_R * CA} \times 100 \quad \text{S13}$$

References

[1] H. Zhang, G. Lin, J. Chen. Evaluation and calculation on the efficiency of a water electrolysis system for hydrogen production. International journal of hydrogen Energy 35 (2010) 10851-10858.

[2] G. Chisholm. L. Cronin. Chapter 16 - Hydrogen From Water Electrolysis. Storing Energy (With Special Reference to Renewable Energy Sources) (2016) 315-343.

[3] S. Pascuzzi, A. S. Anifantis, I. Blanco and G. S. Mugnozza. Electrolyzer Performance Analysis of an Integrated Hydrogen Power System for Greenhouse Heating. A Case Study. Sustainability 8 (2016) 629

[4] M. Hammoudi, C. Henao, K. Agbossou, Y. Dubé, M. L. Doumbia. New multi-physics approach for modelling and design of alkaline electrolyzers. Int. J. Hydrog. Energy 2012, 37, 13895–13913.

[5] H. Ganjehsarabi. Performance assessment of solar-powered high pressure proton exchange membrane electrolyzer: A case study for Erzincan. International journal of hydrogen energy 44 (2019) 9701-9707.

[6] H. Görgün. Dynamic modelling of a proton exchange membrane (PEM) electrolyzer. International Journal of Hydrogen Energy 31 (2006) 29 - 38.

[7] F. M. Nafchi, E. Baniasadi, E. Afshari,N.Javani. Performance assessment of a solar hydrogen and electricity production plant using high temperature PEM electrolyzer and energy storage. International Journal of Hydrogen Energy 43 (2018) 5820-5831.

[8] J. Yu, G. Jung, Y. Su , C. Yeh , M. Kan , C. Lee, C. Lai. Proton exchange membrane water electrolysis system membrane electrode assembly with additive. International Journal of Hydrogen Energy 2019;44:15721-15726.

[9] I. Papagiannakis. Studying and improving the efficiency of water electrolysis using a proton exchange membrane electrolyser. Strathclyde University: 2005, p 57-68.

[10] M. E. Argun, S. Dursun, M. Karata. Removal of Cd(II), Pb(II), Cu(II) and Ni(II) from water using modified pine bark. Desalination 249 (2009) 519-527.

[11] L. Chupin, C. Motillon, F. C. Bouhtoury, A. Pizzi, B. Charrier. Characterisation of maritime pine (Pinus pinaster) bark tannins extracted under different conditions by spectroscopic methods, FTIR and HPLC. Industrial Crops and Products 49 (2013) 897- 903.

[12] A. L. Arim, K. Neves. M. J. Quina, L. M. Gando-Ferreir. Experimental and mathematical modelling of Cr(III) sorption in fixed-bed column using modified pine bark. Journal of cleaner production 183 (2018) 272-281.

[13] A. L. Arim, M. J. Quina, L. M. Gando-Ferreira. Uptake of trivalent chromium from aqueous solutions by xanthate pine bark: Characterization, batch and column studies. Process Safety and Environmental Protection 121 (2019) 374-386.

[14] A. Gundogdu, D. Ozdes, C. Duran, V. N. Bulut, M. Soylak, H. B. Senturk. Biosorption of Pb(II) ions from aqueous solution by pine bark (Pinus brutia Ten.). Chemical Engineering Journal 153 (2009) 62–69.

[15] Y. Zhao, N. Yan, M. W. Feng. Thermal degradation characteristics of phenol-formaldehyde resins derived from beetle infested pine barks. Thermochimica Acta 555 (2013) 46-5.

[16] N. A. H. Rosli, K. S. Loh, W. Y. Wong, T. K. Lee and A. Ahmad. Hybrid Composite Membrane of Phosphorylated Chitosan/Poly (Vinyl Alcohol)/Silica as a Proton Exchange Membrane. Membranes 11 (2021) 675.

[17] H. Toribio-Cuaya, L. Pedraza-Segura, S. Macías-Bravo, I. Gonzalez-García, R. Vasquez-Medrano, E. Favela-Torres. Characterization of Lignocellulosic Biomass Using Five Simple Steps. JCBPS; Section D: Dev. of Biotechno. Process; Special Issue; 4 (2014) 28-47.

[18] F. Rahmawati, A. F. Ridassepri, Chairunnisa, A. T. Wijayanta, K. Nakabayashi, J. Miyawaki, T. Miyazaki. Carbon from Bagasse Activated with Water Vapor and Its Adsorption Performance for Methylene Blue. Appl. Sci. 2021, 11, 678.

[19] M. M. Gomaa, C. Hugenschmidt, M. Dickmann, E. E. Abdel-Hady, H. F. M. Mohamed and M. O. Abdel-Hamed. Crosslinked PVA/SSA proton exchange membranes: correlation between physiochemical properties and free volume determined by positron annihilation spectroscopy. Phys. Chem. Chem. Phys., 20 (2018) 28287-28299.

[20] K. S. W. Sing, D. H. Everett, R. A. W. Haul, L. Moscou, R. A. Pierotti, J. Rouquerol, T. Siemieniewska. Reporting Physisorption Data for Gas/solid Systems with Special Reference to the Determination of Surface Area and Porosity. Pure & App. Chem., 57 (1985) 603-619.

[21] B. Alagappan. Assessing Different Zeolitic Adsorbents for their Potential Use in Kr and Xe Separation. University of Nevada, Las Vegas (2013) 19-25.

[22] M. Thommes, K. Kaneko, A. V. Neimark, J. P. Olivier, F. Rodriguez-Reinoso, J. Rouquerol and K. S. W. Sing. Physisorption of gases, with special reference to the evaluation of surface area and pore size distribution (IUPAC Technical Report). Pure Appl. Chem. 87 (2015) 1051-1069.

[23] A. A. Sapalidis, F. K. Katsaros, and N. K. Kanellopoulos. PVA / Montmorillonite Nanocomposites: Development and Properties in Nanocomposites and Polymers with Analytical Methods. London, United Kingdom: IntechOpen, 2011 [Online]. Available: https://www.intechopen.com/chapters/17185 doi: 10.5772/18217.

[24] C. Liu, C. Dai, C. Chao, S. Chang. Novel proton exchange membrane based on crosslinked poly (vinyl alcohol) for direct methanol fuel cells. Journal of Power Sources 249 (2014) 285-298.

[25] D. Ebenezer, A. P. Deshpande, P. Haridoss. Cross-linked poly (vinyl alcohol)/sulfosuccinic acid polymer as an electrolyte/electrode material for H_2-O_2 proton exchange membrane fuel cells. Journal of Power Sources 304 (2016) 282-292.

[26] M. F. A. Kamaroddin, N. Sabli, P. M. Nia, T. A. T. Abdullah, L. C. Abdullah, S. Izhar, A. Ripin, A. Ahmad. Phosphoric acid doped composite proton exchange membrane for hydrogen production in medium temperature copper chloride electrolysis. International journal of hydrogen energy 45 (2020) 22209-22222.

[27] T. Kamjornsupamitr, T. Sangthumchai, S. Youngme, S. Martwiset. Proton conducting composite membranes from crosslinked poly(vinyl alcohol) and poly(styrenesulfonic acid)-functionalized silica nanoparticles. International journal of hydrogen energy 43 (2018) 1119 0-11201.

[28] J. Rhim, H. B. Park, C. Lee, J. Jun, D. S. Kim, Y. M. Lee. Crosslinked poly(vinyl alcohol) membranes containing sulfonic acid group: proton and

443 methanol transport through membranes. Journal of Membrane Science 238
444 (2004) 143–151.

445 [29] S. Tasarin, C. Panawong, J. Sumranjit, S. Budsombat. Enhancement of
446 proton conductivity of crosslinked poly(vinyl alcohol) through introduction
447 of zeolitic imidazolate framework-8 and imidazole. International journal of
448 hydrogen energy 46 (2021) 36969-36981.

449 [30] L. Zhu, Y. Li, J. Liu, J. He, L. Wang, J. Lei. Recent developments in
450 high-performance Nafion membranes for hydrogen fuel cells applications.
451 Petroleum Science 19 (2022) 1371-1381.

452 [31] J. E. Park, J. Kim, J. Han, K. Kim, S. Park, S. Kim, H. S. Park, Y. Cho,
453 J. Lee, Y. Sung. High-performance proton-exchange membrane water
454 electrolysis using a sulfonated poly(arylene ether sulfone) membrane and
455 ionomer. Journal of Membrane Science 620 (2021) 118871.

456 [32] D. J. Kim, M. J. Jo, S. Y. Nam. A review of polymer-nanocomposite
457 electrolyte membranes for fuel cell application. Journal of Industrial and
458 Engineering Chemistry 21 (2015) 36-52.

459 [33] K. Charradi. Z. Ahmed, R. E. Cid, P. Aranda, E. Ruiz-Hitzky, P. Ocon,
460 R. Chtourou. Amelioration of PEMFC performance at high temperature by
461 incorporation of nanofiller (sepiolite/layered double hydroxide) in Nafion
462 membrane. International Journal of Hydrogen Energy 44 (2019) 10666-
463 10676.

464 [34] H. C. Lee, H. S. Hong, Y. Kim, S. H. Choi, M. Z. Hong, H. S. Lee, K.
465 Kim. Preparation and evaluation of sulfonated-fluorinated poly (arylene
466 ether)s membranes for a proton exchange membrane fuel cell (PEMFC).
467 Electrochimica Acta 49 (2004) 2315–2323.

468 [35] M. Nishihara, Y. Terayama, T. Haji, S. M. Lyth, S. Satokawa, H.
469 Matsumoto. Proton-conductive nano zeolite-PVA composite film as a new
470 water-absorbing electrolyte for water electrolysis. eXPRESS Polymer
471 Letters Vol.12, No.3 (2018) 256-264.

472 [36] P. Kulasekaran, B. M. Mahimai, P. Deivanayagam. Novel cross-linked
473 poly(vinyl alcohol)-based electrolyte membranes for fuel cell applications.
474 RSC Adv. 10 (2020) 26521-26527.

[37] L. M. T. Duarte, G. M. D. Almaraz, C. J. T. Pacheco. Fatigue tests on the proton exchange membrane Nafion 115 (perfluorosulfonic acid) of fuel cells, under the biaxial modality: Tension and torsion. Materials Science for Energy Technologies 2 (2019) 22-28.

[38] J. S. Artimani, M. Arjomand, M. Enhessari, M. Javanbakht. Proton Conducting Nanocomposite Membranes Based on Poly Vinyl Alcohol (PVA) / Glutaraldehyde (GA) for Proton Exchange Membrane Fuel Cells. Iran. J. Chem. Chem. Eng. 40 (2021).

[39] B. Zhou, H. Pu, H. Pan, D. Wan. Proton exchange membranes based on semi-interpenetrating polymer networks of Nafion and poly(vinylidene fluoride) via radiation crosslinking. Internationational Journal of Hydrogen Energy 36 (2011) 6809-6816.

[40] E. Hago and X. Li. Interpenetrating Polymer Network Hydrogels Based on Gelatin and PVA by Biocompatible Approaches: Synthesis and Characterization. Advances in Materials Science and Engineering. 2013, 32876.

[41] J. Y. Yoon, H. Zhang, Y. K. Kim, D. Harbottle, J. W. Lee. A high-strength polyvinyl alcohol hydrogel membrane crosslinked by sulfosuccinic acid for strontium removal via filtration. Journal of Environmental Chemical Engineering 7 (2019) 102824.

[42] M. Kurniati, I. Nuraini, and C. Winarti. Investigation of Swelling Ratio and Textures Analysis of Acrylamide-Nanocellulose Corncobs Hydrogel. Journal of Physics: Conference Series 1805 (2021) 012036.

[43] A. Elzubair, J. C. M. Suarez, C. M. C. Bonelli, E. B. Mano. Gel fraction measurements in gamma-irradiated ultra high molecular weight polyethylene.Polymer Testing 22 (2003) 647-649

[44] F. Gulenoor, P. Poddar, M. D. I. Bossunia, N. C. Dafader, A. M. S. Chowdhury. γ-Irradiated Polyvinyl Alcohol (PVA) and Citric Acid Blend Hydrogels: Swelling and Absorption Properties. Chem Sci J 7 (2016) 1000125.

[45] S. J. Peighambardoust, S. Rowshanzamir, M. Amjadi. Review of the proton exchange membranes for fuel cell applications. International Journal of Hydrogen Energy 35 (2010) 9348-9384.

[46] J. Luo, S. Lindsey. The use of pine bark and natural zeolite as biofilter media to remove animal rendering process odours. Bioresource Technology 97 (2006) 1461-1469.

[47] T. Liu, X. Hui, W. Zhou, Y. Xiao, B. Tang, H. Xiao, J. Lv , L. Xi, G. Li. Dynamics of airborne bacterial community during biofiltration of gases from a swine house. Science of the Total Environment 740 (2020) 139898.

[48] R. Gloukhovski, V. Freger and Y. Tsur. Understanding methods of preparation and characterization of pore-filling polymer composites for proton exchange membranes: a beginner's guide. Rev Chem Eng 2018; 34(4): 455-479.

[49] T. L. Eberhardt, X. Li, T. F. Shupe and C. Y. Hse. Chinese tallow tree (Sapiumsebiferum) utilization: Characterization of extractives and cell-wall chemistry. Wood and Fiber Science 39 (2007) pp 319-324.

[50] X. Yang, H. Pan, T. Zeng, T. F. Shupe, C. Hse. Extraction and Characterization of Seed Oil from Naturally Grown Chinese Tallow Trees. J Am Oil Chem Soc (2013) 90:459-466.

[51] S. Su, Q. Shen, S. Wang, G. Song. Discovery, disassembly, depolymerization and derivatization of catechyl lignin in Chinese tallow seed coats. International Journal of Biological Macromolecules. 239 (2023) 124256.

[52] D. Peterson, J. Vickers, D. DeSantis. Hydrogen Production Cost From PEM Electrolysis. DOE Hydrogen and Fuel Cells Program Record (2020) 19009.

[53] Y. Wang, C. Wen, J. Tu, Z. Zhan, B. Zhang, Q. Liu, Z. Zhang, H. Hu, T. Liu. The multi-scenario projection of cost reduction in hydrogen production by proton exchange membrane (PEM) water electrolysis in the near future (2020–2060) of China. Fuel 354 (2023) 129409.

[54] A. Mayyas, M. Ruth, B. Pivovar, G. Bender, K. Wipke. Manufacturing Cost Analysis for Proton Exchange Membrane Water Electrolyzers. Golden, CO: National Renewable Energy Laboratory. NREL/TP-6A20-72740.

[55] M. J. Ginsberg. Reducing the Production Cost of Hydrogen from Polymer Electrolyte Membrane Electrolyzers through Current Density Operation. Doctoral dissertation, Columbia University (2023) p130.

[56] R. Martinez, E. Forero. Estimation of energy efficiency in solar photovoltaic panels considering environmental variables. IOP Conf. Series: Materials Science and Engineering 437 (2018) 012008.

[57] S. K. Singh, N. Chander. Mid-life degradation evaluation of polycrystalline Si solar photovoltaic modules in a 100 kWp grid-tied system in east-central India. Renewable Energy 199 (2022) 351-367.